

A Non-Equilibrium Sediment Transport Model for Coastal Inlets and Navigation Channels

Alejandro Sanchez[†] and Weiming Wu[‡]

[†]U.S. Army Corps of Engineers Research and Development Center
Coastal and Hydraulics Laboratory
3909 Halls Ferry Road
Vicksburg, MS 39180, USA
Alejandro.Sanchez@usace.army.mil

[‡]University of Mississippi
National Center of Computational Hydroscience and
Engineering
102 Carrier Hall, University, MS, 38677, USA



www.cerf-jcr.org



ABSTRACT

SANCHEZ, A. and WU, W. 2011. A Non-Equilibrium Sediment Transport Model for Coastal Inlets and Navigation Channels. In: Rosati, J.D., Wang, P., and Roberts, T.M. (eds.), *Proceedings, Symposium to Honor Dr. Nicholas C. Kraus*, Journal of Coastal Research, Special Issue, No. 59. West Palm Beach (Florida), ISSN 0729-0208.

This paper presents a depth-averaged sediment transport model with emphasis on morphodynamic processes near coastal inlets and navigation channels. The model solves the depth-averaged two-dimensional non-equilibrium transport equation of total-load sediment, considering bed-material hiding and exposure, avalanching and sediment transport over hard bottoms. The model is coupled with a depth-averaged circulation model and a spectral wave transformation model. Predicted bed changes are compared with measurements for two laboratory experiments of channel infilling and in a field study at Shinnecock Inlet, Long Island, NY. The results indicate that the model is capable of predicting the general trends of morphology change and provides a useful tool for engineering applications such as coastal sediment management, navigation channel maintenance, and beach erosion protection.

ADDITIONAL INDEX WORDS: *Sediment transport, coastal inlet, channel infilling, finite volume, numerical model.*

INTRODUCTION

Coastal inlets are vital navigation links and central for exchange of water, sediment, and nutrients between estuaries and the ocean. Because of the multiple interacting forces (waves, wind, tide, river flows, density currents, etc.) on a wide range of spatial and temporal scales, the complex physical processes of coastal inlets are quantitatively not well understood. Prediction of the morphodynamic processes at coastal inlets has been a challenging, but crucial task for coastal sediment management, navigation channel maintenance, and beach erosion protection. Numerous computational models have been developed in recent decades for this purpose, from one-dimensional (1-D) longshore coastline models, two-dimensional (2-D) cross-shore coastal profile models, 2-D horizontal morphological models to fully three-dimensional local morphological models. Intercomparisons of various morphodynamic models have been made by de Vriend et al. (1993) and Nicholson et al. (1997).

Most coastal sediment transport numerical models are based on the assumption that the bed load or the total load (both bed and suspended loads) are instantaneously in equilibrium on each computational node, calculate the transport rate using empirical formulas, and then determine the bed change by solving the sediment balance equation or the Exner (1925) equation (e.g.,

Stuikma et al. 1985; Chesher et al., 1993; Roelvink and Banning 1994; Ranasinghe et al. 1999; Cayocca 2001; Fortunato and Oliveira, 2003; Buttolph et al. 2006; Warner et al., 2008). Such models are referred to as equilibrium or saturated transport modeling. However, because of the dynamic nature of currents and waves on the coast, neither bed load nor suspended load are usually in an equilibrium state. The assumption of local equilibrium may lead to unrealistic results and instabilities that can mask the morphodynamic bed change and limit long-term simulations. In order to reduce instabilities, filtering procedures and/or diffusive numerical schemes have been commonly implemented in some of these models (e.g., Johnson and Zyserman, 2002), but such procedures are without physical basis.

A more realistic modeling approach for sediment transport is the non-equilibrium transport model, which has been widely used in river sedimentation (e.g., Han 1980; Phillips and Sutherland, 1989; and Wu 2004). This approach renounces the assumption of local equilibrium and solves the actual transport equations for bed and suspended loads; thus, it describes the temporal and spatial lags between flow and sediment transport. Compared to equilibrium formulations, the non-equilibrium sediment transport model is usually more stable and can more easily describe over- and under-loading as well as hard (nonerodible) bottoms.

The aim of this paper is to describe a non-equilibrium transport model of total-load sediment for the calculation of morphology change under waves and currents at coastal inlets and navigation channels. Presented in this paper are the

governing equations, numerical implementation, and validations of the developed model.

BRIEF DESCRIPTION OF THE COASTAL MODELING SYSTEM

The Coastal Modeling System (CMS), developed under the U. S. Army Corps of Engineers' Coastal Inlets Research Program, is designed for practical applications in navigation channel performance evaluation and sediment management for coastal inlets and adjacent beaches to optimize limited federal channel operation and maintenance funds. The CMS is intended as a research and engineering tool that can be operated by novice and experienced modelers on desk-top computers and can be also run in parallel using OpenMP. The CMS takes advantage of the Surface-water Modeling System (SMS) interface for grid generation and model setup, as well as for plotting and post-processing (Zundel, 2000).

The circulation model in the CMS (called CMS-Flow) computes the unsteady water level and current velocity fields by solving the depth-averaged 2-D shallow water flow equations on a non-uniform Cartesian grid with an explicit finite volume scheme. The model can simulate tide, wind and wave driven currents, and includes the Coriolis force, wind stress, bottom friction, and wave radiation stresses. The primary variables are defined on a staggered grid with water surface level calculated at cell centers and the x - and y -components of the velocity at the left and bottom faces of cells, respectively. Further details of the flow model can be found in Buttolph et al. (2006).

The spectral wave transformation model used in the CMS (called CMS-Wave) solves the steady-state wave-action balance equation on a non-uniform Cartesian grid with a finite difference scheme. It considers wind wave generation and growth, diffraction, reflection, dissipation due to bottom friction, white capping and breaking, wave-wave and wave-current interactions, wave runup, wave setup, and wave transmission through structures. The wave diffraction is based on the parabolic wave approximation equation suggested by Mase et al. (2005). CMS-Wave is a half-plane model based on the assumption that waves propagate from the offshore boundary towards shore. Reflected waves are calculated with a backward marching routine. Further information on the wave model can be found in Mase et al. (2005) and Lin et al. (2008).

The existing sediment transport model in the CMS has two options. One option is a total-load formulation that solves the Exner equation for bed change, and the other option solves the suspended-load transport (advection-diffusion) equation and the bed-load mass balance equation (Buttolph et al. 2006). Both options pertain to the equilibrium transport model. To enhance the performance of the CMS, the non-equilibrium sediment transport model is implemented in this study. The methodologies and merits of this model are described in the following sections.

NEWLY DEVELOPED SEDIMENT TRANSPORT MODEL

Total Load Sediment Transport Equation

The moving sediment (total load) in the water column is traditionally divided to suspended load and bed load. The bed load moves by rolling, sliding and saltating in a thin layer of a few particle sizes above the bed, whereas the suspended load is transported by the turbulent flow in the water column above the bed-load layer. Integrating the 3-D sediment transport equation over the suspended-load layer yields the governing advection-diffusion (A-D) equation for suspended load in tensor notation (Wu, 2007):

$$\frac{\partial}{\partial t} \left(\frac{hC}{\beta_s} \right) + \frac{\partial (U_j h C)}{\partial x_j} = \frac{\partial}{\partial x_j} \left[v_s h \frac{\partial C}{\partial x_j} \right] + P - D \quad (1)$$

where t is the time, x_j is the horizontal coordinate with subscript $j=1$ and 2, U_j is the depth-averaged current velocity in the j -th direction, h is the total water depth, C is the depth-averaged suspended-load concentration, β_s is a suspended-load correction factor, v_s is the sediment diffusion coefficient, and P and D are the entrainment and deposition rates of sediment at the interface between bed and suspended loads, respectively. The depth-averaged suspended-load concentration used here is defined as $C = [(h-a)U_s]^{-1} \int_a^h u_s c dz$, where c is the local sediment concentration, a is the thickness of the bed-load layer, u_s is the stream-wise local current velocity, and U_s is the stream-wise depth-averaged velocity approximated as the depth-averaged resultant $U_c = \sqrt{U_x^2 + U_y^2}$. With this definition, the suspended sediment transport is simply $q_{sj} = U_j h C$. The suspended-load correction factor is given by $\beta_s = \int_a^h u_s c dz / (U_c \int c dz)$, which accounts for the time lag (hysteresis) between flow and suspended sediment transport and has a value close to unity for fine sediments, but decreases with increasing grain size (Wu et al. 2006). The sediment diffusion coefficient is assumed to be proportional to the turbulent eddy viscosity as $v_s = \nu_t / \sigma_s$, in which σ_s is the Schmidt number (set to 1.0 here).

Similarly, the bed-load transport equation is obtained by integrating the 3-D sediment transport equation over the bed-load layer as follows (Wu, 2007):

$$\frac{\partial}{\partial t} \left(\frac{q_b}{u_b} \right) - (1 - p_m) \frac{\partial \zeta}{\partial t} + \frac{\partial (\alpha_{bj} q_b)}{\partial x_j} = D - P \quad (2)$$

where p_m is the bed sediment porosity, ζ is the still-water depth, q_b is the bed-load transport rate, u_b is the bed-load velocity, and α_{bj} is the bed-load transport direction cosine coefficient.

Defining the total-load transport rate as $q_{tj} = \alpha_{bj} q_b + U_j h C$, and summing Equations (1) and (2) leads to the overall sediment balance equation:

$$\frac{\partial}{\partial t} \left(\frac{hC_t}{\beta_t} \right) - (1 - p_m) \frac{\partial \zeta}{\partial t} + \frac{\partial q_{ij}}{\partial x_j} = \frac{\partial}{\partial x_j} \left[v_s h \frac{\partial C}{\partial x_j} \right] \quad (3)$$

where C_t is the depth-averaged total-load sediment concentration $C_t = q_t / (U_c h)$, and β_t is the total-load correction factor related to β_s , U_c and u_b as follows (Wu, 2007):

$$\beta_t = \frac{1}{r_s / \beta_s + (1 - r_s) U_c / u_b} \quad (4)$$

where r_s is the fraction of suspended load in total load. Similar to β_s , β_t accounts for the time lag between flow and sediment transport. Because there is no direct solution for β_t , it must be calculated iteratively; thus, for practical applications, its value may be interpolated from a pre-computed table or set to a constant for a certain range of field conditions (set to 0.7 here).

To close the sediment transport model, the second term on the left-hand side of Equation (3) is substituted with the non-equilibrium relation for bed change suggested by Wu (2004):

$$(1 - p_m) \frac{\partial \zeta}{\partial t} = \frac{1}{L_t} (q_{t^*} - q_t) \quad (5)$$

where q_t and q_{t^*} are the actual and equilibrium total-load transport rates, and L_t is the adaptation length or characteristic distance for sediment to adjust from non-equilibrium (i.e. $q_t \neq q_{t^*}$) to equilibrium. The equilibrium transport rate may be calculated from empirical sediment transport formulas. In the CMS, the user has the option to choose from the following three transport equations: Lund-CIRP (Carmenen and Larson 2007), Watanabe (1987), or van Rijn (2007a, b). Equation (5) is referred to as the bed change equation.

By temporarily ignoring the bed-slope effect on the bed-load transport direction and setting $\alpha_{ij} = U_j / U_c$, the total-load transport can be written as $q_{ij} = U_j h C_t$. Inserting this expression and Equation (5) into (3) leads to the following sediment transport equation:

$$\frac{\partial}{\partial t} \left(\frac{hC_t}{\beta_t} \right) + \frac{\partial (U_j h C_t)}{\partial x_j} = \frac{\partial}{\partial x_j} \left[v_s h \frac{\partial (r_s C_t)}{\partial x_j} \right] + \alpha_t \omega_f (C_{t^*} - C_t) \quad (6)$$

where ω_f is the sediment fall velocity, C_{t^*} is the depth-averaged total-load concentration at the equilibrium state, and $\alpha_t = U_c h / (L_t \omega_f)$ is the total-load adaptation coefficient.

Equation (6) is used in this study for sediment transport calculation. It is closed by assuming $r_s = C_s^* / C_{t^*}$, in which C_s^* is the depth-averaged suspended-load concentration at the equilibrium state. The fraction r_s is determined with the van Rijn sediment transport capacity equations. The advantage of

this total-load formulation is that the suspended- and bed-load transport equations are combined into a single equation and there is only one empirical parameter (α_t or L_t) to estimate.

Sediment Adaptation Length

The adaptation length is an important parameter in the developed sediment transport model. Because the total load is a combination of the bed and suspended loads, its adaptation length may be calculated as $L_t = r_s L_s + (1 - r_s) L_b$ or $L_t = \max(L_s, L_b)$, where L_s and L_b are the suspended- and bed-load adaptation lengths. L_s is defined as $L_s = U_c h / (\alpha \omega_f)$, where α is the adaptation coefficient for suspended load. There are several expressions in the literature for calculating α , either empirical such as Lin (1984) or based on analytical solutions to the pure vertical convection-diffusion equation of suspended sediment such as Armanini and di Silvio (1986) and Zhou and Lin (1998). The bed-load adaptation length L_b may be related to the dimension of bed forms such as sand dunes. However, although there is some guidance on ways to estimate L_t its determination is still empirical and in the developmental stage. For further discussion of the adaptation length, see Wu (2007). At the present time, it is recommended that the adaptation length be examined with field data on morphology change or channel infilling to obtain the best and most reliable result.

Bed Slope Effect

The influence of bed slope on morphology change is considered by an additional term in the bed change equation:

$$(1 - p_m) \frac{\partial \zeta}{\partial t} = \alpha_t \omega_f (C_{t^*} - C_t) + \frac{\partial}{\partial x_j} \left[D_s |U_c| h (1 - r_s) C_t \frac{\partial \zeta}{\partial x_j} \right] \quad (7)$$

where D_s is an empirical coefficient. The last term in Equation (7) is a bed-slope term. This term was first applied by Watanabe (1985) and Stuiksma et al. (1985), also in a total-load formulation in which the transport was assumed to be bed-load dominant and therefore $r_s \approx 0$. Watanabe (1985) used $D_s = 10$ for stability reasons, whereas Stuiksma et al. (1985) used $D_s = 4$. Later studies such as Larson et al. (2003) and Karambas (2003) reported good results with $D_s = 2$. In the present model, a default value of 1 is implemented to avoid over-smoothing the morphology change. In practice D_s may be a function of the flow and sediment characteristics and vary from site to site.

Hiding and Exposure

In many locations on the coast, the bed material is dominated by a single sediment size with patches of other sediment sizes or materials (e.g., shell hash), which do not contribute significantly to morphology change at specific regions, but do modify the sediment transport through hiding and exposure. For example, it

is common for the bed material to have a bimodal distribution with a second peak corresponding to local patches of coarser material consisting mostly of shell fragments. The shell material is difficult to model numerically because it is usually poorly sorted and its hydraulic properties are still largely unknown. Sediment transport models commonly estimate excessive erosion in these areas because of ignoring the hiding effect of the coarser shell material (e.g., Cayocca 2001).

The hiding and exposure mechanism is considered in the present model by correcting the critical Shields parameter as $\Theta_{ck}^{he} = \xi_k \Theta_{ck}$, in which ξ_k is the dimensionless hiding and exposure correction function, Θ_{ck} is the critical Shields parameter of the transport grain size d_k , and Θ_{ck}^{he} is the corrected critical Shields parameter. The correction function of Parker et al. (1992) and others is used, i.e., $\xi_k = (d_k / d_{50})^{-m}$ where d_{50} is the bed-material median size and m is an empirical coefficient between 0.5 and 1.0 (set here to 0.7). The aforementioned sediment transport capacity equations are implemented by specifying the transport grain size d_k rather than the bed-material d_{50} . A single, constant transport size d_k is used, while the bed-material d_{50} varies spatially. The spatial distribution of d_{50} can be obtained from measurements, and for simplicity is assumed constant in time in this study. It is noted that the best hiding and exposure function may depend on the chosen transport equations and sediment characteristics. However, this method provides a simple conceptual mechanism for considering an important process in a single-sized sediment transport model.

Avalanching

If the slope of a non-cohesive bed ϕ_i becomes larger than the angle of repose ϕ_r , the bed material will slide (avalanche) to form a new slope approximately equal to the angle of repose. The process of avalanching is simulated by enforcing $|\phi_i| \leq \phi_r$, while maintaining mass continuity between adjacent cells. The following equation for bed change due to avalanching is obtained by combining the equation of angle of repose and the continuity equation between two adjacent cells and summing over all neighboring cells of p :

$$\Delta \zeta_p^a = R \sum_i \frac{A_i \delta x_i (\tan \phi_i - \text{sgn} \phi_i \tan \phi_r)}{A_p + A_i} H(|\phi_i| - \phi_r) \quad (8)$$

where δx_i is the cell center distance between cells p and i , A is the cell area, R is an under-relaxation factor (approximately 0.25-0.5), and $H(X)$ is the Heaviside step function representing the activation of avalanching and equal to 1 for $X > 0$ and 0 for $X \leq 0$. The sign function $\text{sgn} X$ is equal to 1 for $X > 0$ and -1 for $X < 0$ and accounts for the fact that the bed slope may have a negative or positive sign.

Equation (8) is applied by sweeping through all computational cells to calculate $\Delta \zeta^a$ and then modifying the bathymetry as $\zeta^{n+1} = \zeta^n + \Delta \zeta^a$. Because avalanching between two cells may induce new avalanching at neighboring cells, the sweeping process is repeated until no avalanching occurs. The under-relaxation coefficient R stabilizes the avalanching process and eliminates overshooting since the equation is derived considering only two adjacent cells, but is summed over all (avalanching) neighboring cells. Equation (8) may be applied to any grid geometry type (triangles, rectangles, etc.), and also in situations where neighboring cells are joined at corners without sharing a cell face.

Hardbottom

Equation (5) and in turn (6) are based on the assumption of the existence of a loose or movable bottom in which the bed material is available for entrainment. Sometimes one may encounter hard bottoms where bed materials are nonerodible, such as bare rocks and concrete structures. The hard-bottom cells are treated simply by modifying the equilibrium concentration as $C_{i*}' = \min(C_{i*}, C_i)$ in both the transport and bed-change equations. The bed-slope term in Equation (7) is also modified, so that only deposition occurs at hard-bottom cells.

Boundary Conditions

The sediment flux between dry and wet cells is assigned to zero. Outflow boundaries are assigned a zero-gradient boundary condition for sediment concentration. Inflow boundaries may be assigned a specific concentration, the equilibrium concentration, or a zero-gradient in the sediment concentration.

NUMERICAL IMPLEMENTATION AND COMPUTATION PROCEDURE

The governing equations (6) and (7) are discretized using the Finite Volume Method on a non-uniform Cartesian grid. The advection terms are discretized with the second-order Hybrid Linear/Parabolic Approximation (HLPA) scheme of Zhu (1991), and the diffusion and bed slope terms are discretized with the standard central difference scheme. Time integration is performed with the explicit Euler scheme. The bed- and suspended-load equilibrium sediment transport rates can be multiplied by user-specified scaling factors. The scaling factors are intended for calibration purposes and have a typical range between 0.5-2.0. Unless specified otherwise, the transport scaling factors are equal to 1.0 (default value). The bed change can also be multiplied by a morphologic scaling factor at every time step, to speed up the morphologic modeling of bed evolution under cyclic or steady flow conditions (Lesser et al. 2004). However, this factor was not used in the results presented in this paper.

The flow, waves, and morphology change are dynamically coupled. The wave model is run first for one wave steering interval. The wave heights, periods, directions, and radiation

stress gradients are then passed to the flow and sediment transport models by means of communication files and the wave variables are interpolated onto the flow grid. Once the flow and sediment transport models have reached the end of the wave steering interval, the wave model is run again and the process is repeated. The wave and flow models may have different computational grids, while the flow and sediment transport models occupy the same grid. The flow and sediment transport may also have different time steps. During the calculation of sediment transport, the bed elevation is updated and passed to the flow model at every sediment time step, which the wave model also accesses. For typical coastal applications, a wave steering interval of 1-3 hr is used, and flow and sediment time steps are typically about 1 and 10 s, respectively.

MODEL COMPARISON WITH LABORATORY DATA

Case 1: Channel infilling under cross-channel flow with parallel waves

A laboratory experiment on the evolution of channel morphology under cross-channel flow with waves parallel to the channel axis was carried out in a wave-current flume by van Rijn and Havinga (1995). The channel was approximately 4 m wide and 0.22 m deep, and had 1:10 side slopes (see Figure 1). The current speed at the inflow boundary was 0.245 m/s. Incident irregular waves (JONSWAP form) were parallel to the channel axis (90° with respect to the flow) and had a significant wave height of 0.105 m and peak wave period of 2.2 s. The initial bathymetric profile is shown in Figure 1. Manning's coefficient n is calibrated as approximately 0.02 with the measured velocity profile. The bed slope coefficient is set to 2.0. The sediment median diameter d_{50} is 0.1 mm. The transport grain size is set to d_{50} , so that no hiding and exposure is considered. The sediment concentration at the inflow boundary is specified as the equilibrium concentration based on the Lund-CIRP transport equations. The total load adaptation length calibrated as 0.75 m by comparing the calculated and measured morphology changes.

The computed morphology change is found to agree well with the measured, as shown in Figure 1. The root-mean-squared error (RMSE) between measured and computed water depths is 0.01 m, less than 5% of the upstream flow depth. The relative-mean-absolute error (RMAE) is 2%. The model reproduced well the general trend of the morphology change including the upstream bank migration and downstream bank erosion. The small oscillations (on the order of 1 m in length) in the measured bathymetry are more likely to be large bed forms that are not simulated in the present model.

Case 2: Channel infilling under cross-channel flow with perpendicular waves

A laboratory experiment on the channel morphology change under cross-channel flow with waves perpendicular to the channel axis was carried out by van Rijn (1985). The rectangular experiment flume was 17 m long and 0.3 m wide. The channel had a side slope of 1:10 and a depth of 0.125 m with respect to the sides. The water depth and current velocity at the upstream

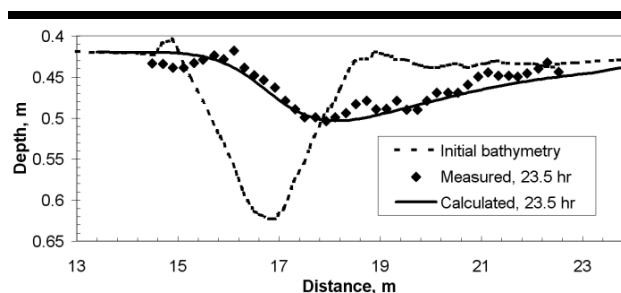


Figure 1. Comparison of measured and calculated water depths for case 1.

end of the flume were 0.255 m and 0.18 m/s, respectively. Regular waves were generated in the same direction of the flow with a height of 0.08 m and period of 1.5 s. The movable bed consisted of fine sand ($d_{50} = 0.1$ mm). The measured suspended sediment transport at the upstream end of the flume was 0.0167 kg/m-s. For further details on the experiment, see van Rijn (1985, 1986).

The suspended sediment transport capacity was calculated with the Lund-CIRP transport equation calibrated to match the inflow transport by multiplying a correction factor equal to 0.8. This factor is within the generally accepted range of 0.5-2. Since no measurements for bed load are available, the bed-load transport capacity is not modified. As in the previous case, the transport grain size is set to d_{50} so that no hiding and exposure was represented. The bed slope coefficient was set to 1.0. The adaptation length is calibrated as approximately 2.5 m by comparing the measured and calculated morphologic changes. Figure 2 shows a comparison of the measured and computed bed elevations after 10 hrs. The model reproduced well the overall trend channel infilling, but slightly underestimated the upstream bank migration and slightly overestimated downstream bank erosion. The RMSE and RMAE for Case 2 are 0.01 m and 3%, respectively.

MODEL APPLICATION AT SHINNECOCK INLET, NY

Background

Shinnecock Inlet is the eastern-most permanent inlet on Long Island, NY (see Figure 3). During the Great New England storm on September 21, 1938, the barrier island was breached and the inlet entrance began to grow (Morang, 1999). The inlet was stabilized in the 1950s with two rubble mound jetties. It is a mixed-energy, wave dominated inlet. The tide is mainly semi-diurnal with an average spring tidal range of 1.1 m. Shinnecock Bay has water depths typically less than 2 m and a tidal prism of 3.29×10^7 m³ (Militello and Kraus, 2001). The bay is connected to Moriches Bay to the west through the Quogue and Quantuck Canals and to Peconic Bay to the north through the Shinnecock Canal. Several small creeks drain a small amount of freshwater into the bay. The beach to the west of the inlet, called Tiana Beach, experiences chronic erosion and

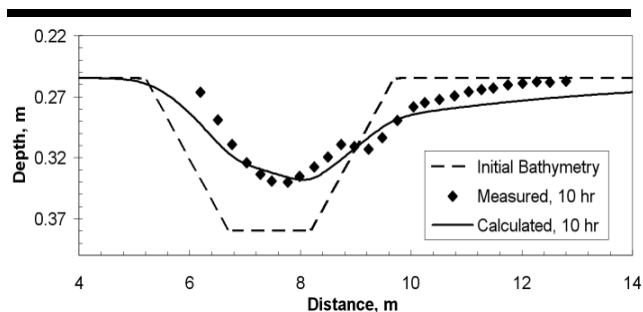


Figure 2. Comparison of measured and calculated water depths for case 2.

is typically nourished with sediment dredged from the navigation channel deposition basin located just outside of the inlet. Typical wave conditions are from the southeast with wave heights of 1 m and periods of 7 s, while northeast storms and hurricanes can produce wave heights in excess of 4 m with periods of 12-14 s (Buonaiuto and Militello 2003).

Estimated net longshore transport rates vary significantly depending on the year. Rosati, et al. (1999) conducted a thorough sediment budget considering shoreline change, dredging, beach nourishment, and possible onshore transport and estimated a long-term net alongshore rate of $150,000 \pm 40,000 \text{ yd}^3/\text{yr}$. The ratio between the tidal prism and net longshore sediment transport suggests that the sediment bypassing occurs due to a combination of tidal bypassing and wave induced currents (Buonaiuto and Militello 2004).

Model Setup

The simulation covers the time period between August 13, 1997 and May 28, 1998 (approximately 9.5 months), which corresponds to the dates of LIDAR surveys with no dredging activity in between. The model bathymetry is generated by blending SHOALS LIDAR data (Lillycrop et al. 1996), the National Geophysical Data Center Coastal Relief Model (NGDC, 2009), and single beam surveys done by the USACE and Stony Brook University, NY. The computational grid and initial bathymetry are shown in Figure 4. The grid for flow computation has 49,780 cells and a variable grid resolution between 15 and 100 m. The CMS-Wave and CMS-Flow grids are identical except that the wave grid does not include the inner bay beyond the flood shoal where wave heights are negligible. A sensitivity analysis by Militello and Kraus (2001) showed that the canals and creeks connecting to Shinnecock Bay may be ignored in modeling the tidal inlet, and are therefore not included in this present simulation.

Wind data were obtained from the National Climatic Data Center Blended Sea Winds (NCEP, 2009). The wind data set consists of 6-hr wind fields on a global 0.25° grid. The dataset wind speeds are generated by blending observations from several satellites including QuikSCAT, and the wind directions are interpolated from the NCEP Re-analysis 2 (NRA-2) dataset.

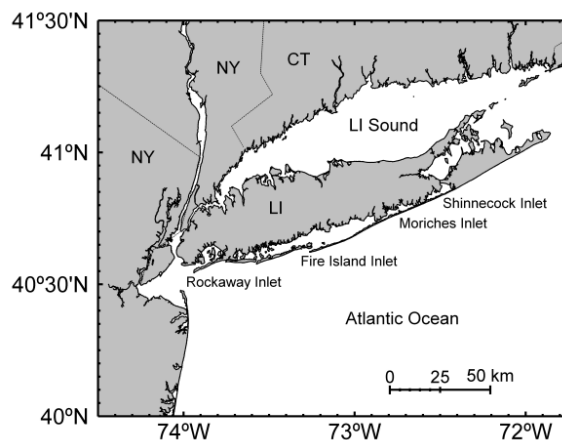


Figure 3. Location of Shinnecock Inlet.

The offshore boundary is forced with a predicted water surface elevation computed from a 3-yr harmonic analysis of a pressure gauge record (P1) located just outside of the inlet (see Militello and Kraus, 2001 for more details). The harmonic analysis includes twelve major constituents. The computed amplitudes of the four major constituents are: M2 of 0.48 m, N2 of 0.11 m, S2 of 0.10 m, and K1 of 0.08 m. The fitted harmonic prediction represents 90% of the water level variance. The remaining 10% variance consists mostly of high frequency (supertidal) water level fluctuations induced by local wind and waves and should not be included at the offshore boundary.

Directional wave spectra are obtained at 3-hr intervals from the National Data Buoy Center (NDBC) station 44025 located 33 nautical miles off the coast of Long Island. The offshore spectra are transformed to the offshore CMS-Wave boundary by assuming straight contours parallel to the shoreline. The wave steering interval is 3 hr.

The spatial distribution of the grain sediment size (d_{50}) is obtained from Pratt and Stauble (2001). The sediment grain size varies significantly spatially from 0.125 mm offshore and inside the bay to 2.0 mm in the inlet. Based on grain size analysis by Pratt and Stauble (2001), the dominate grain size for the ebb shoal (area of interest) is approximately 0.5 mm. Therefore, 0.5 mm is used as the transport grain size d_k . Although the sediment samples were taken during July of 1998, it is assumed that they are representative of the simulation period. The inlet is well known to have hard, compacted sands with large amounts of shell hash that prevents the main channel from eroding. Therefore, a constant hard bottom 1 m below the initial bed elevation is set at the inlet to avoid excessive erosion.

The concentration capacity is calculated with Watanabe (1987) transport equation with a transport coefficient 0.25. The adaptation length is given as 20 m, and the bed slope coefficient is 1.0. Since the Watanabe (1987) transport equation does not provide information on the fraction of suspended sediments, this information is calculated with the van Rijn (2007a, b) transport equations.

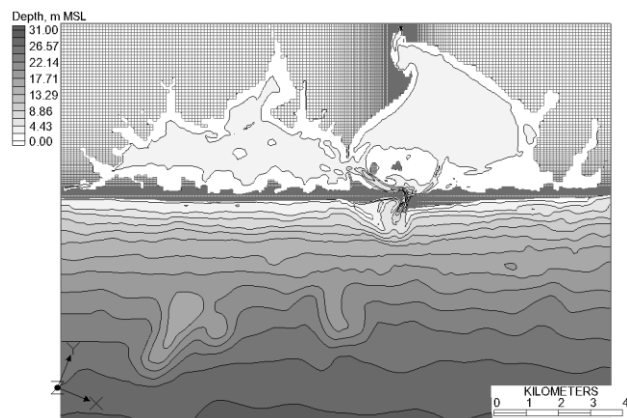


Figure 4. Computational grid with initial bathymetry for 1997. Square cells represent inactive land cells.

Hydrodynamics

The hydrodynamic model is validated by comparing measured and calculated currents and water levels during June 1998 (see Figure 5). The water level station P3 is located at the entrance of Shinnecock Canal which connects Shinnecock Bay to the Great Peconic Bay to the north. The current station C1 is located near the western jetties. Computed water elevations at P3 agree well with measurements. The RMSE and RMAE are 0.03 m and 0.11, respectively. The computed current velocities at C1 are not as good as the water surface elevations. Peak flood velocities are underestimated by 5–40%. This is possibly due to secondary currents and three-dimensional processes in the inlet that are not captured by the depth-averaged model. The current RMSE and RMAE are 0.18 m/s and 0.30, respectively. Similar levels of error were obtained by Militello and Kraus (2001) with a finite element model.

Longshore Sediment Transport

As a first measure of how the model represents the nearshore sediment transport processes, the longshore sediment transport rate is calculated by integrating the hourly total-load transport vector field along a transect to the east of the inlet and oriented normal to the shoreline to a depth of about 10 m. The calculated longshore sediment transport rate is 133,000 yd³/yr, which is within the range of 110,000–190,000 yd³/yr reported by Rosati, et al. (1999).

Morphology Change

For brevity, this paper focuses on the morphology change of the ebb shoal. Figures 6 and 7 show the measured and computed morphology for the simulation period. Qualitatively, the results show several features in common such as deposition on the peripheral of the ebb shoal, erosion at both the east bypass bar

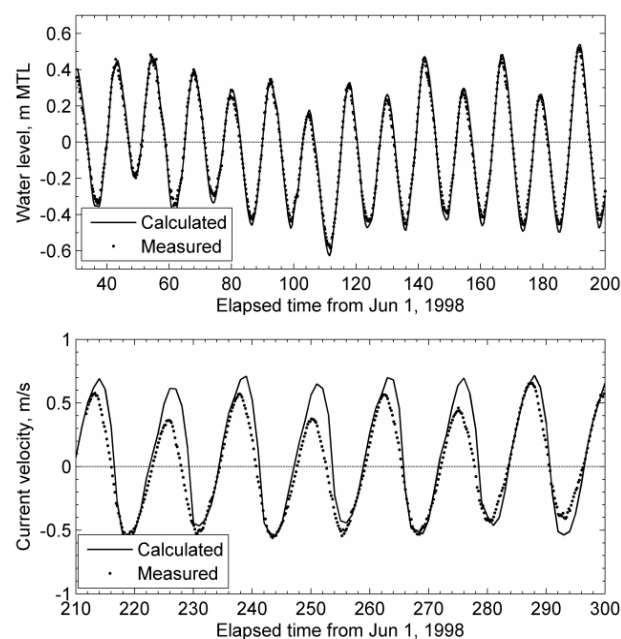


Figure 5. Comparison between measured and computed water levels at stations P3 and C1. Positive current velocities are in the flood direction (north).

and west bypass bars, erosion of the eastern portion of the south bypass bar, and accretion in the deposition basin. Quantitatively, the morphodynamic model accurately predicts either an erosional or depositional trend at approximately 66% of the computational cells. The RMSE and RMAE for the water depth over the ebb shoal complex are 1.1 m and 19% respectively. However, due to the complex nature of the field site, in comparison with the laboratory cases, simply calculating goodness-of-fit statistics from computed and measured water depths may not accurately represent the model skill.

Another way of comparing the computed and measured morphology change is through sediment volume changes for representative morphologic features or regions. For example, the calculated and measured sediment depositions along the peripheral of the ebb shoal are approximately 365,000 and 308,000 m³, respectively. The accretion in the deposition basin is calculated as 184,000 m³, which agrees well to the measured 180,000 m³. The erosion of the west bypass bar is also predicted well at approximately 60,000 m³. The major areas of discrepancy are the overestimation of erosion on the south and east bypass bars, as well as large amounts of accretion in front of Tiana beach, which is not observed in the measurements. The erosion on the east bypass bar is estimated at 230,000 m³ while the measured is only 22,000 m³. The estimated erosion of the south bypass bar is 419,000 m³, while the measured is approximately half at 181,000 m³. The extra sediment eroded from the south bypass bar is deposited in front of Tiana beach,

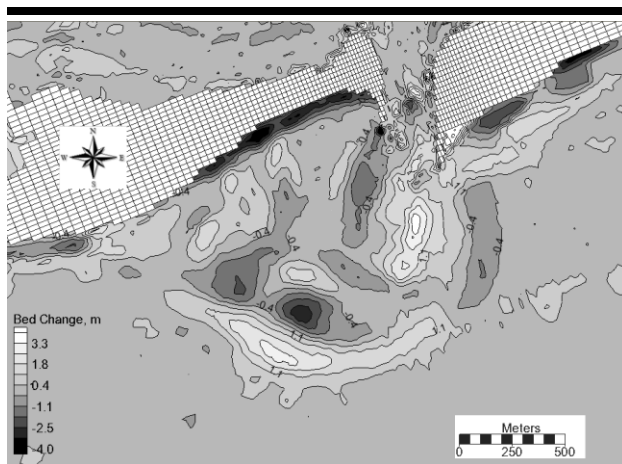


Figure 6. Measured morphology change between August 1997 and May 1998.

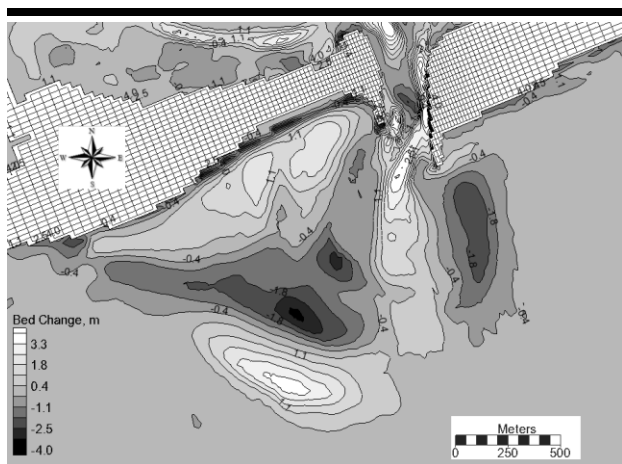


Figure 7. Calculated morphology change between August 1997 and May 1998.

which accounts for the large accretion in this area at $315,000 \text{ m}^3$, while the measured accretion is only $76,000 \text{ m}^3$.

DISCUSSION AND CONCLUSIONS

A new non-equilibrium total-load sediment transport model has been established with emphasis on practical engineering applications at coastal inlets and navigation channels. The governing equations consist of a total-load transport equation and a bed change equation which includes a bed-slope effect term. The model takes into account bed-material hiding and exposure, avalanching, and sediment transport over non-erodible bottoms. The governing equations are solved with an explicit, finite volume scheme on a non-uniform Cartesian grid. The

proposed non-equilibrium sediment transport model is attractive for practical engineering applications because of its simplicity. The bed- and suspended-load transport equations are combined, and therefore, there is one less partial differential equation to be solved. The short-term channel infilling and migration in two laboratory flumes and the mid-term (9.5 month) morphology change at a coastal inlet (Shinnecock Inlet, NY) are reasonably simulated using the CMS with the newly developed sediment model.

Although both flume experiments shared similar characteristics in dimensions, sediment properties, and flow conditions, the calibrated adaptation length is approximately 3 times larger for the case with waves perpendicular to the channel axis (Case 2) compared to the case with waves parallel to the channel axis. This may be related to the direction of the waves or the presence of bed forms in Case 1. It is apparent that more research is needed to predict the adaptation length in the presence of waves. However, once the adaptation length is properly calibrated, excellent results of channel infilling are obtained for both cases.

The calculated 9.5-month morphology changes at Shinnecock Inlet, NY show relatively good agreement with field data. Possible sources of error include boundary conditions, ambiguity in model forcing, empirical sediment parameters, and assumptions in the flow and sediment transport equations. Although not shown, the morphology changes calculated with the Lund-CIRP and van Rijn formulas were remarkably different from the above results obtained with the Watanabe formula. This disparity emphasizes the large error associated with the empirical equations of sediment transport capacity.

Another source of error is the assumption that the net sediment transport is in the direction of the depth-averaged current velocity. The transport equation (6) in the proposed model represents the advection and diffusion of the current-related total-load sediment transport, including wave stirring (additional suspension due to waves). It assumes that sediment advection is solely in the direction of the depth-averaged current velocity and ignores the sediment transport component in the direction of waves due to asymmetrical oscillatory flow near bottom in the presence of shoaling waves (see Ribberink and al Salem 1994; Dohmen-Janssen et al. 2002; Carmenen and Larson, 2007). In the surf zone, this process is responsible for onshore and offshore sediment transport and essential for describing several nearshore morphologic features such as bypass bars. However, inclusion of the wave-related sediment transport is still in the development stage. This model limitation will be addressed in future research.

A major assumption in calculating the hiding and exposure factor is that the spatial distribution of the bed-material d_{50} remains constant in time. The validity of this assumption depends on the specific site and the time scale under consideration. It is reasonable for Shinnecock Inlet, NY in the time period simulated. This assumption is not needed if the present single-sized model is extended to a multiple-sized one in which the time-varying bed-material composition can be calculated directly, as described in Wu (2007). Such a multiple-sized sediment transport model is under development in the CMS in order to simulate long-term morphology changes more realistically.

ACKNOWLEDGMENTS

This work was conducted in part through funding from the Coastal Modeling System work unit of the Coastal Inlets Research Program (CIRP) of the U.S. Army Corps of Engineers. Permission was granted by the Chief, U. S. Army Corps of Engineers, to publish this information. We appreciate the help and support of Dr. Nicholas C. Kraus, Dr. Julie D. Rosati, Dr. Lihwa Lin, Mr. Mitch Brown, Dr. Alan Zundel, and others in CIRP group.

LITERATURE CITED

- Armanini, A., and di Silvio, G., 1986. Discussion on the paper 'A depth-averaged model for suspended sediment transport' by Galappatti, G., and Vreugdenhil, C. B. *Journal of Hydraulic Research*. 24(5), 437-441.
- Buonaiuto, F. S., and Militello, A., 2003. Coupled circulation, wave, and morphology-change modeling, Shinnecock Inlet, New York. Proceedings 8th Conference on Estuarine and Coastal Modeling. ASCE, New York. 819-838.
- Buttolph, A. M.; Reed, C. W.; Kraus, N. C.; Ono, N.; Larson, M.; Carmenen, B.; Hanson, H.; Wamsley, T., and Zundel, A. K., 2006. Two-dimensional depth-averaged circulation model CMS-M2D: Version 3.0, Report 2: Sediment transport and morphology change. Coastal and Hydraulics Laboratory Technical Report ERDC/CHL TR-06-9. Vicksburg, MS: U.S. Army Engineer Research and Development Center, U.S.A.
- Carmenen, B. and Larson, M., 2007. A unified sediment transport formulation for coastal inlet application. Coastal and Hydraulics Laboratory Technical Report, ERDC-CHL CR-07-01. Vicksburg, MS: U.S. Army Engineer Research and Development Center, U.S.A.
- Cayocca, F., 2001. *Long-term morphological modeling of a tidal inlet: the Arcachon Basin, France*. *Coastal Engineering*. 42, 115-142.
- Chesher, T. J.; Wallace, H. M.; Meadowcroft, I. C.; and Southgate, H. N., 1993. Pisces, A Morphodynamic Coastal Area Model. First Annual Report, HR Wallingford Report SR 337, April 1993.
- de Vriend, H. J.; Zyserman, J.; Nicholson, J.; Roelvink, J. A.; Pechon, P., and Southgate, N. H., 1993. Medium term 2DH coastal area modelling. *Coastal Engineering*. 21, 193-224.
- Dohmen-Janssen, C. M.; Kroekenstoel, D.; Hanes, D. M., and Ribberink, J. S., 2002. Phase lags in oscillatory sheet flow: Experiments and bed load modeling. *Coastal Engineering*. 46(1), 61-87.
- Exner, F. M. 1925. *Über die Wechselwirkung zwischen Wasser und Geschiebe in Flüssen*, Sitzber. Akad. Wiss Wien, Part IIa, Bd 134. (In German)
- Fortunato, A. B., and Oliveira, A., 2003. A modeling system for tidally driven long-term morphodynamics. *Journal of Hydraulic Research*. 42(4), 626-634.
- Han, Q. W., 1980. A study of non-equilibrium transportation of suspended load. *Proceedings of the First Symposium on River Sedimentation*. Beijing, China.
- Johnson, H. K., and Zyserman, J. A., 2002. Controlling spatial oscillations in bed level update schemes. *Coastal Engineering*. 46, 109-126.
- Karambas, T. V., 2003. Nonlinear wave modeling and sediment transport in the surf and swash zone. *Advances in Coastal Modeling*, V.C. Lakhan (ed.), Elsevier Oceanography Series, 67, Amsterdam, The Netherlands, 267-298.
- Larson, M.; Hanson, H., and Kraus, N. C., 2003. Numerical modeling of beach topography change. *Advances in Coastal Modeling*, V.C. Lakhan (eds.), Elsevier Oceanography Series, 67, Amsterdam, The Netherlands, 337-365.
- Lesser, G.; Roelvink, J. A.; van Kester, J. A. T. M., and Stelling, G. S., 2004. Development and validation of a three-dimensional morphological model. *Coastal Engineering*. 51, 883-915.
- Lillicrop, W. J.; Parson, L. E., and Irish, J. L., 1996. Development and Operation of the SHOALS Airborne Lidar Hydrographic Survey System. *SPIE Selected Papers, Laser Remote Sensing of Natural Waters: From Theory to Practice*, V. I. Feigles, and Y. Kopilevich (eds.), St. Petersburg, Russia, 2694, 26-37.
- Lin, L.; Demirbilek, Z.; Mase, H.; Zheng, J., and Yamada, F., 2008. CMS-Wave: A nearshore spectral wave processes model for coastal inlets and navigation projects. Coastal and Hydraulics Laboratory Technical Report ERDC/CHL TR-08-13. Vicksburg, MS: U.S. Army Engineer Research and Development Center, U.S.A.
- Lin, B. N., 1984. Current study of unsteady transport of sediment in China. Proc. Japan-China Bilateral Seminar on River Hydraulics and Engineering Experiences, July, Tokyo-Kyoto-Sapporo, Japan. 337-342.
- Mase, H.; Oki, K.; Hedges, T., and Li, H. J., 2005. Extended energy-balance-equation wave model for multidirectional random wave transformation. *Ocean Engineering*. 32, 961-985.
- Militello, A., and Kraus, N. C., 2001. Shinnecock Inlet, New York, Site Investigation: Report 4, Evaluation of flood and ebb shoal sediment source alternatives for the west of Shinnecock Interim Project, New York. Coastal and Hydraulics Laboratory Technical Report ERDC/CHL TR-CHL-98-32. Vicksburg, MS: U.S. Army Engineer Research and Development Center, U.S.A.
- Morang, A., 1999. Shinnecock Inlet, New York, Site Investigation, Report 1, Morphology and Historical Behavior. Coastal and Hydraulics Laboratory Technical Report ERDC/CHL TR-CHL-98-32. Vicksburg, MS: U.S. Army Engineer Research and Development Center, U.S.A.
- NCDC (National Climatic Data Center). 2009. Blended sea winds. <http://www.ncdc.noaa.gov/oa/rsad/blendedseawinds.html>. (dated December 2008; accessed March 17, 2009)
- NGDC (National Geophysical Data Center). 2009. Coastal Relief Model. <http://www.ngdc.noaa.gov/mgg/coastal/coastal.html>. (dated July 2009; accessed January 20, 2009).
- Nicholson, J.; Brøker, I.; Roelvink, J. A.; Price, D.; Tanguy, J. M., and Moreno, L., 1997. Intercomparison of coastal area morphodynamic models. *Coastal Engineering*, 31, 97-123.
- Parker, G.; Klingeman, P. C., and Mclean, D. G., 1982. Bed load and size distribution in paved gravel-bed streams. *Journal of the Hydraulic Division*. ASCE, 108(4), 544-571.

- Phillips, B. C., and Sutherland, A. J., 1989. Spatial lag effects in bed load sediment transport. *Journal of Hydraulic Research*, 27(1), 115–133.
- Pratt, T. C., and Stauble, D. K., 2001. Shinnecock Inlet, New York, Site Investigation, Report 3, Selected field data report for 1997, 1998, 1999 velocity and sediment surveys. Coastal and Hydraulics Laboratory Technical Report ERDC/CHL TR-CHL-98-32. Vicksburg, MS: U.S. Army Engineer Research and Development Center, U.S.A.
- Ranasinghe, R.; Pattiaratchi, C., and Masselink, G., 1999. A morphodynamic model to simulate the seasonal closure of tidal inlets. *Coastal Engineering*, 37, 1-36.
- Ribberink, J. S., and al Salem, A. A., 1994. Sediment transport in oscillatory boundary layers in cases of rippled beds and sheet flow. *Journal of Geophysical Research*, 99(C6), 707-727.
- Roelvink, J. A., and Banning, G. K. F. M. van. 1994. Design and development of Delft3D and application to coastal morphodynamics. Hydrodynamics '94. Verwey, Minns, Babovic & Maksimovic (eds), Balkema, Rotterdam, 451-455.
- Rosati, J. D.; Gravens, G. W., and Smith, M. B., 1999. Regional sediment budget for Fire Island to Montauk Point, New York, USA. *Proceedings Coastal Sediments '99*, N.C. Kraus, and W.G. McDougal (eds.), ASCE, Reston, VA, 802-817.
- Struiksma, N.; Olewesen, K.W.; Flokstra, C.; and de Vriend, H. J., 1985. Bed deformation in curved alluvial channels. *Journal of Hydraulic Research*, 23(1), 57-79.
- van Rijn, L. C., 1985. Flume experiments of sedimentation in channels by currents and waves. Report S 347-II, Delft Hydraulics laboratory, Delft, Netherlands.
- van Rijn, L. C., 1986. Sedimentation of dredged channels by currents and waves. *Journal of Waterway, Port, Coastal, Ocean Engineering*, 112, 541-559.
- van Rijn, L. C., 2007a. Unified view of sediment transport by currents and waves. I: Initiation of bed motion, bed roughness, and bed-load transport. *Journal of Hydraulic Engineering*, 133(6), 649-667.
- van Rijn, L. C. 2007b. Unified view of sediment transport by currents and waves. II: Suspended transport. *Journal of Hydraulic Engineering*, 133(6), 668-689.
- van Rijn, L. C., and Havinga, F., 1995. Transport on fine sands by currents and waves. Part 2. *Journal of Waterway, Port, Coastal, and Ocean Engineering*, 121(2), 123–133.
- Warner, J. C.; Sherwood, C. R.; Signell, R. P.; Harris, K., and Arango, H. G., 2008. Development of a three-dimensional, regional, coupled wave, current, and sediment-transport model. *Computers and Geosciences*, 34, 1284-1306.
- Watanabe, A., 1985. Three-dimensional predictive model of beach evolution around a structure. *Proceedings of the International Symposium of Water Wave Research*. University of Hannover, Germany, 121-142.
- Watanabe, A., 1987. 3-dimensional numerical model of beach evolution. *Proceedings Coastal Sediments '87*, N.C. Kraus (ed.), ASCE, Reston, VA, 802-817.
- Williams, G.L.; Morang, A., and Lillycrop, L., 1998. Shinnecock Inlet, New York, Site Investigation, Report 2: Evaluation of Sand Bypass Options. Coastal and Hydraulics Laboratory Technical Report ERDC/CHL TR-CHL-98-32. Vicksburg, MS: U.S. Army Engineer Research and Development Center, U.S.A.
- Wu, W., 2004. Depth-averaged two-dimensional numerical modeling of unsteady flow and nonuniform sediment transport in open channels. *Journal of Hydraulic Engineering*, ASCE, 130(10), 1013-1024.
- Wu, W., 2007. Computational River Dynamics. London: Taylor & Francis, pp. 494.
- Wu, W.; Altinakar, M., and Wang, P. 2006. Depth-averaged analysis of hysteresis between flow and sediment transport under unsteady conditions. *International Journal of Sediment Research*, 21(2), 101-112.
- Zhu, J., 1991. A low-diffusive and oscillation-free convection scheme. *Communications in Applied Numerical Methods*, 7, 225-232.
- Zhou, J., and Lin, B., 1998. One-dimensional mathematical model for suspended sediment by lateral integration. *Journal of Hydraulic Engineering*, ASCE, 124(7), 712-717.
- Zundel, A. K., 2000. Surface-water modeling system reference manual. Brigham Young University, Environmental Modeling Research Laboratory, Provo, UT.

NOTATION

C_t [-]	Depth-averaged total-load concentration
C_{rs} [-]	Depth-averaged total-load capacity
C [-]	Depth-averaged suspended-load concentration
D_s [-]	Bed slope coefficient
h [L]	Flow depth
L_t [L]	Total-load adaptation length
p'_m [-]	Bed porosity
q_b [L ² /T]	Bed-load transport
q_s [L ² /T]	Suspended-load transport
q_t [L ² /T]	Total-load transport
u_b [L/T]	Bed-load velocity
U [L/T]	Depth-averaged current velocity
U_c [L/T]	Depth-averaged current magnitude
α_b [-]	Bed-load transport direction cosine coefficient
α_t [-]	Total-load adaptation coefficient
β_s [-]	Suspended-load correction factor
β_t [-]	Total-load correction factor
ζ [L]	Still water depth
ν_s [L ² /T]	Sediment diffusion coefficient
ν_t [L ² /T]	Eddy viscosity
ω_f [L/T]	Settling velocity